Deletion of mitochondrial calcium uniporter incompletely inhibits calcium uptake and induction of the permeability transition pore in brain mitochondria

Received for publication, March 14, 2018, and in revised form, August 22, 2018 Published, Papers in Press, August 28, 2018, DOI 10.1074/jbc.RA118.002926

James Hamilton[‡], Tatiana Brustovetsky[‡], Jacob E. Rysted[§], Zhihong Lin[§], Yuriy M. Usachev[§], and Nickolay Brustovetsky[‡¶1]

From the [‡]Department of Pharmacology and Toxicology and the [¶]Stark Neurosciences Research Institute, Indiana University School of Medicine, Indianapolis, Indiana 46202 and the [§]Department of Pharmacology, University of Iowa Carver College of Medicine, Iowa City, Iowa 52242

Edited by Phyllis I. Hanson

Ca^{2+} influx into mitochondria is mediated by the mitochondrial calcium uniporter (MCU), whose identity was recently revealed as a 40-kDa protein that along with other proteins forms the mitochondrial Ca^{2+} uptake machinery. The MCU is a Ca^{2+}-conducting channel spanning the inner mitochondrial membrane. Here, deletion of the MCU completely inhibited Ca^{2+} uptake in liver, heart, and skeletal muscle mitochondria. However, in brain nonsynaptic and synaptic mitochondria from neuronal somata/glial cells and nerve terminals, respectively, the MCU deletion slowed, but did not completely block, Ca^{2+} uptake. Under resting conditions, brain MCU-KO mitochondria remained polarized, and in brain MCU-KO mitochondria, the electrophoretic Ca^{2+} ionophore ETH129 significantly accelerated Ca^{2+} uptake. The residual Ca^{2+} uptake in brain MCU-KO mitochondria was insensitive to inhibitors of mitochondrial Na^+/Ca^{2+} exchanger and ryanodine receptor (CGP37157 and dantrolene, respectively), but was blocked by the MCU inhibitor Ru360. Respiration of WT and MCU-KO brain mitochondria was similar except that for mitochondria that oxidized pyruvate and malate, Ca^{2+} more strongly inhibited respiration in WT than in MCU-KO mitochondria. Of note, the MCU deletion significantly attenuated but did not completely prevent induction of the permeability transition pore (PTP) in brain mitochondria. Expression level of cyclophilin D and ATP content in mitochondria, two factors that modulate PTP induction, were unaffected by MCU-KO, whereas ADP was lower in MCU-KO than in WT brain mitochondria. Our results suggest the presence of an MCU-independent Ca^{2+} uptake pathway in brain mitochondria that mediates residual Ca^{2+} influx and induction of PTP in a fraction of the mitochondrial population.

Mitochondrial Ca^{2+} uptake and the ability of Ca^{2+} to regulate mitochondrial functions have been established for many years (1–4). Ca^{2+} uptake by mitochondria plays an important role for the organelle and for the whole cell. It helps to maintain low cytosolic Ca^{2+} when Ca^{2+} influx into the cell is increased (*e.g.* following stimulation of ionotropic glutamate receptors in neurons) (5–7). The delivery of Ca^{2+} into the mitochondrial matrix can activate mitochondrial dehydrogenases such as pyruvate, α-ketoglutarate, and isocitrate dehydrogenases and, thereby, can stimulate mitochondrial respiration and ATP production (4). Finally, excessive Ca^{2+} uptake may lead to mitochondrial damage through induction of the permeability transition pore (PTP)[2] (3, 8). Ca^{2+} transport into mitochondria is mediated by the Ca^{2+} uniporter, a Ca^{2+} channel complex in the inner mitochondrial membrane (9, 10), the molecular identity of which was recently revealed (11, 12).

In recent studies, it was found that mitochondria contain several proteins involved in Ca^{2+} transport into the organelle: MCU (mitochondrial calcium uniporter) (11, 13), MCUb (14), MICU1 and MICU2 (15–17), EMRE (18), and MCUR (19). Among other components of mitochondrial Ca^{2+} transport machinery, MCU is believed to be the Ca^{2+} channel traversing the inner mitochondrial membrane (IMM) (13). In experiments with purified MCU reconstituted into a planar bilayer, ruthenium red, an inhibitor of the Ca^{2+} uniporter (20, 21), blocked MCU-mediated Ca^{2+} currents (11). Genetic ablation of MCU completely prevented Ca^{2+} uptake by skeletal muscle and heart mitochondria and inhibited induction of the PTP but failed to protect cells from cell death and failed to protect cardiac tissue from ischemia–reperfusion injury (22).

The Ca^{2+}-dependent induction of the PTP is the major mechanism of Ca^{2+}-induced mitochondrial damage (3, 8, 23, 24). In the brain, PTP induction and consequent mitochondrial damage are the primary mechanisms contributing to glutamate

This work was supported by National Institutes of Health Grants R01 NS087068 and R01 NS096246 (to Y. U.) and R01 NS098772 (to N. B.). This study was supported in part by a grant from the Indiana Traumatic Spinal Cord & Brain Injury Research Fund (to N. B.). The authors declare that they have no conflicts of interest with the contents of this article. The content is solely the responsibility of the authors and does not necessarily represent the official views of the National Institutes of Health.

[1] To whom correspondence should be addressed: Dept. of Pharmacology and Toxicology, Indiana University School of Medicine, 635 Barnhill Dr., Medical Science Bldg., Rm. 547, Indianapolis, IN 46202. Tel.: 317-278-9229; Fax: 317-274-7714; E-mail: nbrous@iu.edu.

[2] The abbreviations used are: PTP, permeability transition pore; MCU, mitochondrial calcium uniporter; CyD, cyclophilin D; CsA, cyclosporin A; 2,4-DNP, 2,4-dinitrophenol; TPP^+, tetraphenylphosphonium; IMM, inner mitochondrial membrane; mNCX, mitochondrial Na^+/Ca^{2+} exchanger; mRR, mitochondrial ryanodine receptor; NMDA, *N*-methyl-D-aspartate; FCCP, carbonyl cyanide *p*-trifluoromethoxyphenylhydrazone; Cyt *c*, cytochrome *c*; VDAC1, voltage-dependent anion channel 1; BisTris, 2-[bis(2-hydroxyethyl)amino]-2-(hydroxymethyl)propane-1,3-diol; KO, knockout.

excitotoxicity (25–27), a major deleterious factor in stroke, secondary traumatic brain injury, and various neurodegenerations. An induction of the PTP requires Ca^{2+} influx into mitochondria (28). Correspondingly, knockdown of MCU reduced NMDA-induced increases in mitochondrial Ca^{2+} in neurons, leading to milder mitochondrial depolarization and elevated resistance to excitotoxicity (29). On the other hand, MCU KO failed to protect brain from hypoxic-ischemic damage, despite strongly hindering mitochondrial Ca^{2+} uptake and PTP induction (30).

One reason for this controversy could be an incomplete inhibition of Ca^{2+} uptake in brain mitochondria from MCU-KO mice. However, brain mitochondria from MCU-KO mice are poorly characterized in terms of Ca^{2+} uptake, membrane potential changes, respiratory activities, and susceptibility to PTP induction. In the present study, we investigated the effect of MCU KO on Ca^{2+} uptake and membrane potential in isolated brain nonsynaptic and synaptic mitochondria as well as in liver, heart, and skeletal muscle mitochondria. We also compared respiratory activities of brain mitochondria isolated from WT and MCU-KO mice. Finally, we evaluated susceptibility of MCU-KO and WT mitochondria to PTP induction. Our results demonstrate that there is a unique MCU-independent, Ru360-sensitive Ca^{2+} uptake in brain mitochondria that results in PTP induction in a fraction of vulnerable organelles. Thus, these findings evince a potential mechanism by which deletion of MCU might be not very efficacious in protecting brain mitochondria from PTP induction and, consequently, in protecting the brain from ischemia–reperfusion insults.

Results

The effect of MCU deletion on mitochondrial Ca^{2+} uptake

All MCU-KO mice used in our experiments were genotyped (Fig. 1*A*) and all mitochondrial preparations were tested for MCU by immunoblotting (Fig. 1*B*). The level of MCU expression in brain nonsynaptic mitochondria of MCU-KO mice was below the detection limit of Western blotting. Expression of MCU paralog, MCUb (18), was slightly but statistically significantly lower in brain nonsynaptic mitochondria from MCU-KO mice compared with mitochondria from WT animals. In our study, we used a high-resolution Ca^{2+}-sensitive electrode that enabled us to evaluate, with high precision, changes in the rate of Ca^{2+} uptake by mitochondria from MCU-KO and WT mice. To assess the rate and capacity of Ca^{2+} uptake, multiple pulses of $CaCl_2$ were applied to mitochondria (Fig. 1, *D* and *E*). Mitochondrial Ca^{2+} uptake was monitored by measuring a decrease in external Ca^{2+}. Brain nonsynaptic mitochondria isolated from WT mice accumulated Ca^{2+} faster than mitochondria from MCU-KO animals (Fig. 1*D*). Despite this, Ca^{2+} uptake capacity, determined as the amount of Ca^{2+} accumulated by mitochondria before they failed to accumulate additional Ca^{2+}, was not significantly different. BSA significantly increased the Ca^{2+} uptake capacity (Fig. 1*E*). The Ca^{2+} uptake capacity is limited by an induction of the PTP (30). Because BSA binds free fatty acids (31), which are activators of the PTP (32), its inclusion in the incubation medium defers PTP induction and, consequently, increases

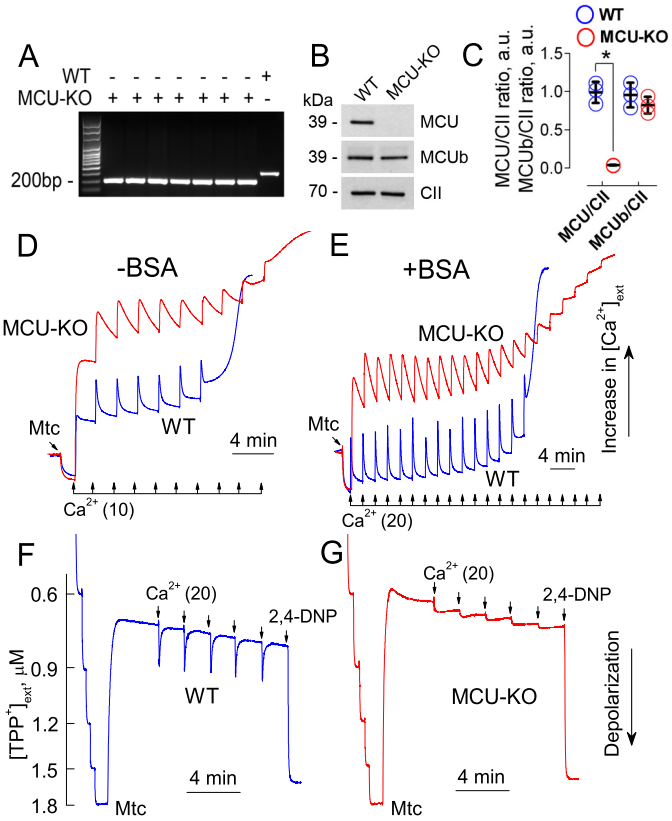

Figure 1. Ca^{2+} uptake and membrane potential in brain nonsynaptic mitochondria from MCU-KO and WT CD1 mice. *A*, representative genotyping data of tail tissue from WT and MCU-KO mice. *B*, Western blotting demonstrating the lack of MCU in brain nonsynaptic mitochondria from MCU-KO mice and the presence of MCUb in mitochondria of WT and MCU-KO animals. A 70-kDa subunit of Complex II (*CII*) was used as a loading control. *C*, statistical analysis of immunoblotting. Data are mean ± S.D. (*error bars*), $n = 3$. *, $p <$ 0.001 comparing MCU/Complex II in WT and MCU-KO mitochondria. *D*, Ca^{2+} uptake by brain mitochondria from WT (*blue trace*) and MCU-KO (*red trace*) mice. Here and in *E*, mitochondria (0.18 mg of protein/ml) were incubated in the standard incubation medium supplemented with 3 mM pyruvate plus 1 mM malate, 0.1 mM ADP, and 1 μM oligomycin. *E*, Ca^{2+} uptake by WT (*blue trace*) and MCU-KO (*red trace*) brain mitochondria incubated in the presence of 0.1% BSA (free from fatty acids). *F* and *G*, the effect of Ca^{2+} on mitochondrial membrane potential in WT and MCU-KO mitochondria, respectively. In these experiments, the standard incubation medium was supplemented with 0.1% BSA (free from fatty acids). *D–G*, Ca^{2+} was added to mitochondria where indicated as 10 or 20 μM $CaCl_2$ pulses, respectively. *Numbers in parentheses* indicate $CaCl_2$ concentrations in μM. *a.u.*, arbitrary units.

Ca^{2+} uptake capacity (33). In the presence of BSA, the Ca^{2+} uptake capacities of MCU-KO and WT mitochondria remain similar (Fig. 1*E*). In parallel experiments, we tested the effect of Ca^{2+} pulses on mitochondrial membrane potential (Fig. 1, *F* and *G*). The decreased rate of Ca^{2+} uptake by MCU-KO mitochondria (Fig. 1, *D* and *E*) could result from these mitochondria being less polarized. However, under resting conditions, mitochondria from MCU-KO and WT mice accumulated comparable amounts of TPP^+, suggesting similar polarization of both MCU-KO and WT mitochondria. The repetitive Ca^{2+} pulses produced fast, transient depolarizations in WT mitochondria (Fig. 1*F*), whereas in MCU-KO mitochondria, Ca^{2+} pulses produced slower depolarizations with much smaller amplitude (Fig. 1*G*). At the end of these experiments, mitochondria were treated with the uncoupler 2,4-dinitrophenol (2,4-DNP) to produce maximal depolarization.

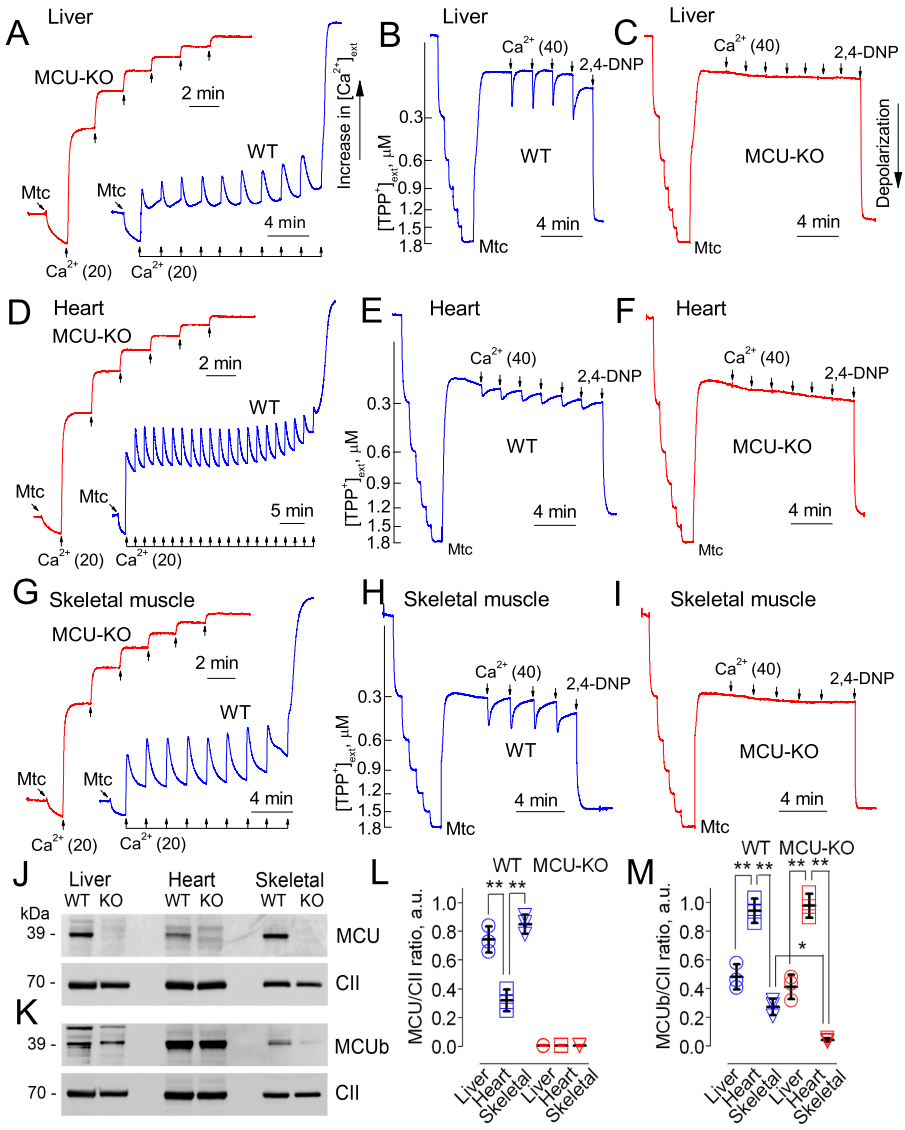

Figure 2. Ca^{2+} uptake and membrane potential in liver (*A–C*), heart (*D–F*), and skeletal muscle (*G–I*) mitochondria from MCU-KO and WT CD1 mice. *A*, Ca^{2+} uptake by liver mitochondria from WT (*blue trace*) and MCU-KO (*red trace*) mice. Note the different time scales for WT and MCU-KO mitochondria in *A*, *D*, and *G*. In *A–C*, liver mitochondria (1.5 mg of protein/ml) were incubated in the standard incubation medium supplemented with 3 mM pyruvate plus 1 mM malate, 0.1 mM ADP, 1 μM oligomycin, 0.1% BSA (free from fatty acids). *B* and *C*, the effect of Ca^{2+} on mitochondrial membrane potential in WT and MCU-KO liver mitochondria, respectively. Where indicated, Ca^{2+} was added to mitochondria as 20 or 40 μM $CaCl_2$ pulses, respectively. Here and in other panels, *numbers* in *parentheses* indicate $CaCl_2$ concentrations in μM. In *B* and *C*, 60 μM 2,4-DNP was used to depolarize mitochondria. *D*, Ca^{2+} uptake by WT (*blue trace*) and MCU-KO (*red trace*) heart mitochondria (0.7 mg of protein/ml) incubated in the same medium as liver mitochondria. In *E* and *F*, the effect of Ca^{2+} on mitochondrial membrane potential in WT and MCU-KO heart mitochondria, respectively. In *E* and *F*, 60 μM 2,4-DNP was used to depolarize mitochondria. In *G*, Ca^{2+} uptake by WT (*blue trace*) and MCU-KO (*red trace*) skeletal muscle mitochondria (1.3 mg of protein/ml) incubated in the same medium as liver mitochondria. *H* and *I*, effect of Ca^{2+} on mitochondrial membrane potential in WT and MCU-KO skeletal muscle mitochondria, respectively. *H* and *I*, 60 μM 2,4-DNP was used to depolarize mitochondria. *J* and *K*, Western blots demonstrating the lack of MCU in mitochondria from MCU-KO mice and the presence of MCUb in mitochondria of WT and MCU-KO animals, respectively. A 70-kDa subunit of Complex II (*CII*) was used as a loading control. In *L* and *M*, statistical analyses of immunoblotting. Data are mean ± S.D. ($n = 3$). *L*, **, $p < 0.001$ comparing MCU/Complex II in heart mitochondria with MCU/Complex II in liver and skeletal muscle mitochondria. *M*, *, $p < 0.05$ comparing MCUb/Complex II in skeletal muscle mitochondria from WT and MCU-KO mice; **, $p < 0.001$ comparing MCU/Complex II in WT or MCU-KO heart mitochondria with WT or MCU-KO liver and skeletal muscle mitochondria. *a.u.*, arbitrary units.

In contrast to brain nonsynaptic mitochondria, mitochondria isolated from liver, heart, and skeletal muscles of MCU-KO mice were not able to take Ca^{2+} up and depolarize in response to Ca^{2+} (Fig. 2). The MCU expression in heart mitochondria was the lowest compared with other tissues (Fig. 2*J*). The level of MCU in mitochondria from MCU-KO mice was below the detection limit of Western blotting. The level of MCUb varied among mitochondria from different tissues, with skeletal muscle mitochondria having the least amount of MCUb and heart mitochondria having the greatest amount of MCUb (Fig. 2*K*). Expression of MCUb was distinctly lower in skeletal muscle mitochondria from MCU-KO mice compared with MCUb level in skeletal muscle mitochondria from WT animals.

ETH129, an electrophoretic Ca^{2+} ionophore (34), can transport Ca^{2+} across the membrane independently of the Ca^{2+} uniporter (35). Ru360, an inhibitor of the Ca^{2+} uniporter (36), strongly inhibited Ca^{2+} uptake (Fig. 3*B*). When the Ca^{2+} uniporter was blocked by Ru360, ETH129 restored Ca^{2+} uptake by brain nonsynaptic mitochondria. Similarly, ETH129 significantly increased Ca^{2+} uptake rate in brain nonsynaptic

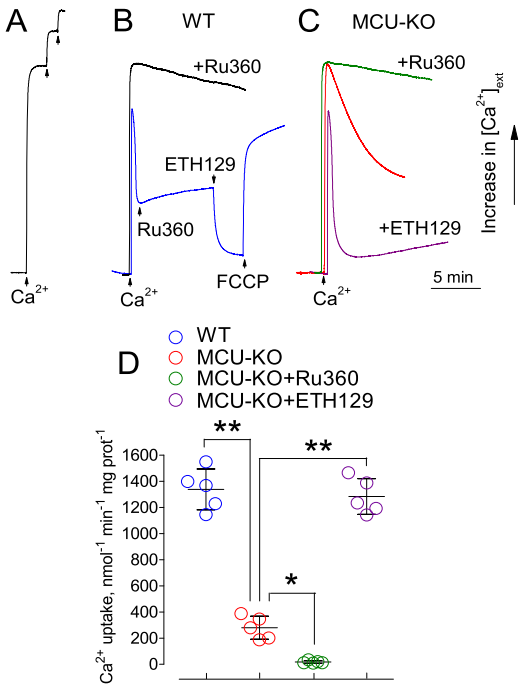

Figure 3. An electrophoretic Ca^{2+} ionophore ETH129 rescues Ca^{2+} uptake by WT brain nonsynaptic mitochondria treated with Ru360 and significantly accelerates Ca^{2+} uptake by MCU-KO mitochondria. Ru360 inhibits residual Ca^{2+} uptake by MCU-KO mitochondria. *A*, calibration of the Ca^{2+}-selective electrode with sequential 100 μM $CaCl_2$ pulses. *B*, inhibition of Ca^{2+} uptake by WT mitochondria with 3.3 μM Ru360 and restoration of Ca^{2+} uptake with 5 μM ETH129. At the end of the experiment, 1 μM FCCP was added to depolarize mitochondria and release accumulated Ca^{2+}. In *C*, acceleration of Ca^{2+} uptake by MCU-KO mitochondria in the presence of 5 μM ETH129. Ru360 (3.3 μM) strongly inhibits Ca^{2+} uptake by MCU-KO mitochondria. In *B* and *C*, Ca^{2+} was added to mitochondria as 100 μM $CaCl_2$ pulses. The *time bar* shown in *C* is also applicable to *A* and *B*. In *D*, statistical analysis of data. Data are shown as mean ± S.D. (*error bars*), $n = 5$. *, $p < 0.05$ comparing rates of Ca^{2+} uptake by MCU-KO mitochondria with and without 3.3 μM Ru360. **, $p < 0.001$ comparing rates of Ca^{2+} uptake by MCU-KO mitochondria *versus* WT mitochondria and MCU-KO mitochondria in the presence of 5 μM ETH129. Here and in other figures, statistical analysis consisted of one-way analysis of variance followed by Bonferroni's post hoc test (GraphPad Prism version 4.0, GraphPad Software).

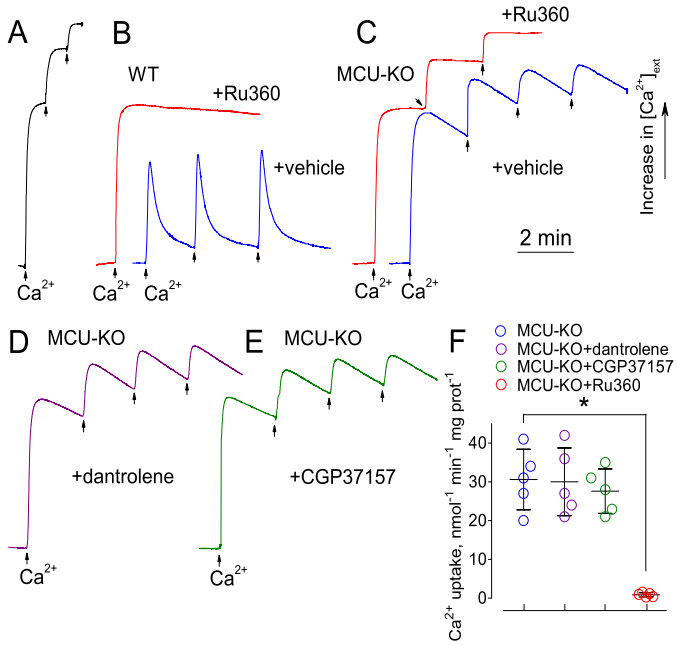

Figure 4. Ca^{2+} uptake by brain nonsynaptic mitochondria from MCU-KO mice: the effects of CGP37157, dantrolene, and Ru360. *A*, calibration of the Ca^{2+}-selective electrode with sequential 20 μM $CaCl_2$ pulses. *B*, Ca^{2+} uptake by WT mitochondria without (*blue trace*) and with 3.3 μM Ru360 (*red trace*). The vehicle was 5 μl of deoxygenated water, which was used to dissolve Ru360. *C*, Ca^{2+} uptake by MCU-KO mitochondria treated with vehicle (*blue trace*) or with 3.3 μM Ru360 (*red trace*). Here and in all other *panels*, Ca^{2+} was added to mitochondria where indicated as 20 μM $CaCl_2$ pulses. In *D* and *E*, the residual Ca^{2+} uptake by MCU-KO mitochondria in the presence of 20 μM dantrolene (*D*) and 10 μM CGP37157 (*E*). In *F*, statistical analysis of Ca^{2+} uptake data. Ca^{2+} uptake rates were quantified as Ca^{2+} uptake per minute per mg of mitochondrial protein. Data are shown as mean ± S.D. (*error bars*) ($n = 5$). *, $p < 0.001$ comparing rates of Ca^{2+} uptake by MCU-KO mitochondria treated with vehicle or Ru360. The *time scale* shown in *C* is applicable to *A*, *B*, *D*, and *E*.

mitochondria from MCU-KO mice (Fig. 3*C*). This is consistent with unaffected polarization of MCU-KO mitochondria and supports the notion that deletion of MCU was the main cause of inhibition of Ca^{2+} uptake. On the other hand, Ru360 strongly inhibited Ca^{2+} uptake by MCU-KO mitochondria (Fig. 3*C*). Fig. 3*D* shows statistical analysis of the data. Fig. 3*A* shows a calibration of the Ca^{2+}-selective electrode with consecutive 100 μM $CaCl_2$ pulses.

The intriguing finding that despite MCU deletion, MCU-KO brain nonsynaptic mitochondria were able to accumulate Ca^{2+} (Fig. 1, *D* and *E*), suggested that either MCU is not a Ca^{2+} channel essential for Ca^{2+} uptake and serves a regulatory role or there are alternative pathways for Ca^{2+} influx into mitochondria. Because reconstituted MCU was able to generate Ca^{2+} currents in experiments with planar lipid bilayer (11), the former hypothesis seems unlikely. The alternative pathways for Ca^{2+} uptake by MCU-KO brain mitochondria could include mitochondrial Na^+/Ca^{2+} exchanger, operating in reverse (37, 38), or ryanodine receptor, found in mitochondria (mRR) (39, 40). However, neither CGP37157, an inhibitor of mitochondrial Na^+/Ca^{2+} exchanger (41), nor dantrolene, an inhibitor of ryanodine receptor that inhibited mRR in previous studies (39, 40), suppressed the residual Ca^{2+} uptake by MCU-KO mitochondria (Fig. 4, *C–F*). Here again, Ru360, strongly inhibited Ca^{2+} uptake by WT and MCU-KO mitochondria (Fig. 4, *B* and *C*). Fig. 4*A* shows calibration of the Ca^{2+}-selective electrode with consecutive 20 μM $CaCl_2$ pulses, whereas Fig. 3*F* shows statistical analysis of these Ca^{2+} uptake experiments. The difference in the rates of Ca^{2+} uptake shown in Figs. 3 and 4 is most likely due to the difference in the concentration of added Ca^{2+}. In Fig. 3, Ca^{2+} uptake was induced by adding 100 μM Ca^{2+}, whereas in Fig. 4, 20 μM Ca^{2+} was added.

The role of MCU in regulation of mitochondrial respiration

In the mitochondrial matrix, Ca^{2+} activates pyruvate dehydrogenase as well as the Krebs cycle enzymes isocitrate dehydrogenase and α-ketoglutarate dehydrogenase (4), and therefore, inhibition of Ca^{2+} influx into mitochondria might affect mitochondrial respiration. To test this possibility, we performed respirometry experiments using a Clark electrode and isolated brain nonsynaptic mitochondria fueled either with pyruvate plus malate (Complex I substrates) (Fig. 5, *A* and *B*) or with succinate (a Complex II substrate) (Fig. 5, *C* and *D*). In the latter case, the incubation medium was supplemented with 3 mM glutamate to remove oxaloacetate in transaminase reaction to prevent oxaloacetate accumulation and inhibition of succinate dehydrogenase (42, 43). We analyzed basal respiration

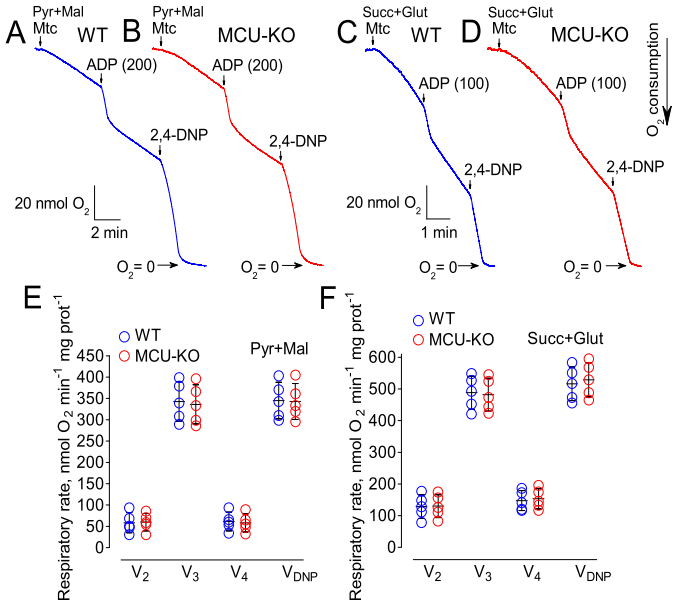

Figure 5. Respiration of brain nonsynaptic mitochondria isolated from WT and MCU-KO mice. In *A* and *B*, respiration of WT and MCU-KO mitochondria, respectively, fueled with a combination of 3 mM pyruvate plus 1 mM malate. Where indicated in *parentheses*, 200 μM ADP was added to mitochondria. At the end of the experiment, 60 μM 2,4-DNP was added to maximally stimulate respiration. In *C* and *D*, respiration of WT and MCU-KO mitochondria, respectively, fueled with a combination of 3 mM succinate plus 3 mM glutamate. Where indicated in *parentheses*, 100 μM ADP was added to mitochondria. At the end of the experiment, 60 μM 2,4-DNP was added to maximally stimulate respiration. In these experiments (*A*–*D*), the standard incubation medium was supplemented with 0.1% BSA (free from fatty acids). In *E* and *F*, statistical analyses of respiratory rates of WT and MCU-KO mitochondria fueled with 3 mM pyruvate plus 1 mM malate (*E*) or 3 mM succinate plus 3 mM glutamate (*F*). V_2, V_3, V_4, and V_{DNP}, respiratory rates before the ADP addition, after the ADP addition, after the depletion of added ADP, and after the addition of 2,4-DNP, respectively. Data are shown as mean ± S.D. (*error bars*), $n = 5$.

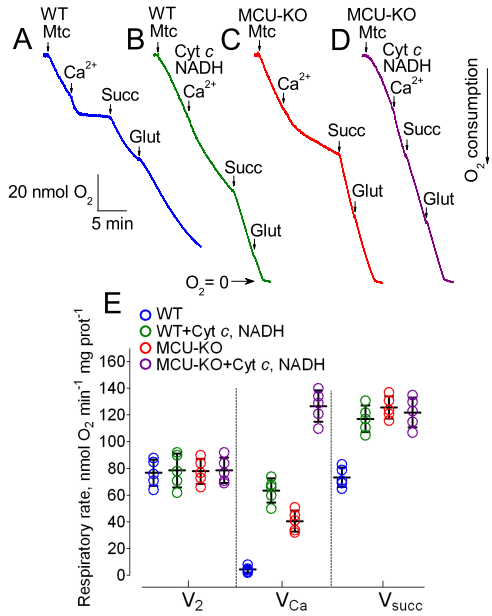

Figure 6. The effect of Ca^{2+} on respiration of brain nonsynaptic mitochondria isolated from WT and MCU-KO mice. In *A*–*D*, respiration of WT and MCU-KO mitochondria was initially fueled with a combination of 3 mM pyruvate plus 1 mM malate. Where indicated, 100 μM $CaCl_2$, 3 mM succinate, or 3 mM glutamate were added to mitochondria. In *B* and *D*, the incubation medium was supplemented with 30 μg/ml Cyt *c* and 3 mM NADH. In *E*, statistical analysis of respiratory rates of WT and MCU-KO mitochondria fueled with 3 mM pyruvate plus 1 mM malate. V_2, V_{Ca}, and V_{Succ}, respiratory rates before the $CaCl_2$ addition, after the $CaCl_2$ addition, and after the addition of succinate, respectively. Data are shown as mean ± S.D. (*error bars*), $n = 5$. $p < 0.001$ comparing V_2 with V_{Ca} and V_{Succ} of MCU-KO mitochondria; comparing V_2 with V_{Ca} of WT mitochondria; comparing V_2 and V_{Succ} of WT mitochondria incubated with Cyt *c* and NADH; comparing V_2 with V_{Ca} and V_{Succ} of MCU-KO mitochondria incubated with Cyt *c* and NADH; comparing V_{Ca} of WT and MCU-KO mitochondria incubated with or without Cyt *c* and NADH; and comparing V_{Succ} of WT and MCU-KO mitochondria.

(V_2), governed predominantly by proton permeability of the IMM; ADP-stimulated respiration (V_3), determined primarily by activity of the oxidative phosphorylation system; the controlled respiration (V_4), determined by proton permeability of the IMM and possible contaminations with ATPase activities; and uncoupled respiration (V_{DNP}), governed by activity of the mitochondrial electron transport chain. In our experiments, we did not find a significant difference in respiration of mitochondria from MCU-KO and WT mice under any tested conditions. Fig. 5 (*E* and *F*) shows statistical analyses of respirometry data. Thus, deletion of MCU does not affect mitochondrial respiration under resting, ADP-stimulated, and uncoupled conditions.

The Ca^{2+} influx into mitochondria may induce the PTP (28), and this may affect mitochondrial respiration (44). Interestingly, this effect depends on the type of oxidative substrates used in these experiments. With WT mitochondria oxidizing pyruvate plus malate, Ca^{2+} produced strong inhibition of respiration that could be rescued by succinate (Fig. 6*A*). Further improvement was achieved by adding a combination of 3 mM NADH and 30 μg/ml cytochrome *c* (Cyt *c*) (Fig. 6*B*). With MCU-KO mitochondria, Ca^{2+}-induced respiratory inhibition was also apparent but was much weaker (Fig. 6*C*). Similar to experiments with WT mitochondria, succinate and Cyt *c* plus NADH improved respiration of MCU-KO mitochondria (Fig. 6*D*), and the effect of succinate was stronger than with WT mitochondria. Glutamate added after succinate failed to further improve mitochondrial respiration (Fig. 6, *A*–*D*). Fig. 6*E* shows statistical analyses of these experiments.

The effect of MCU deletion on PTP opening

The Ca^{2+}-induced inhibition of mitochondrial respiration fueled by Complex I substrates was demonstrated previously (44). This could be explained by an induction of the PTP and loss of mitochondrial NADH (45). On the other hand, stimulation of mitochondrial respiration fueled by succinate was also attributed to PTP induction leading to uncoupling of oxidative phosphorylation and the increased respiratory rate (44). Taken together, the effects of Ca^{2+} on mitochondrial respiration suggested a decreased propensity of MCU-KO mitochondria for PTP induction. To test this hypothesis, we monitored simultaneously changes in light scattering of mitochondrial suspension, indicative of mitochondrial swelling, and distribution of lipophilic cation tetraphenylphosphonium (TPP^+) across the IMM, indicative of changes in mitochondrial membrane potential (Fig. 7). An addition of $CaCl_2$ (100 μM) to WT nonsynaptic mitochondria produced a rapid decrease in light scattering, indicating swelling of the organelles, and an increase of TPP^+ concentration in the incubation medium, indicating mitochondrial depolarization (Fig. 7*A*). To quantify mitochondrial swelling, alamethicin, a pore-forming agent (46), was added to mito-

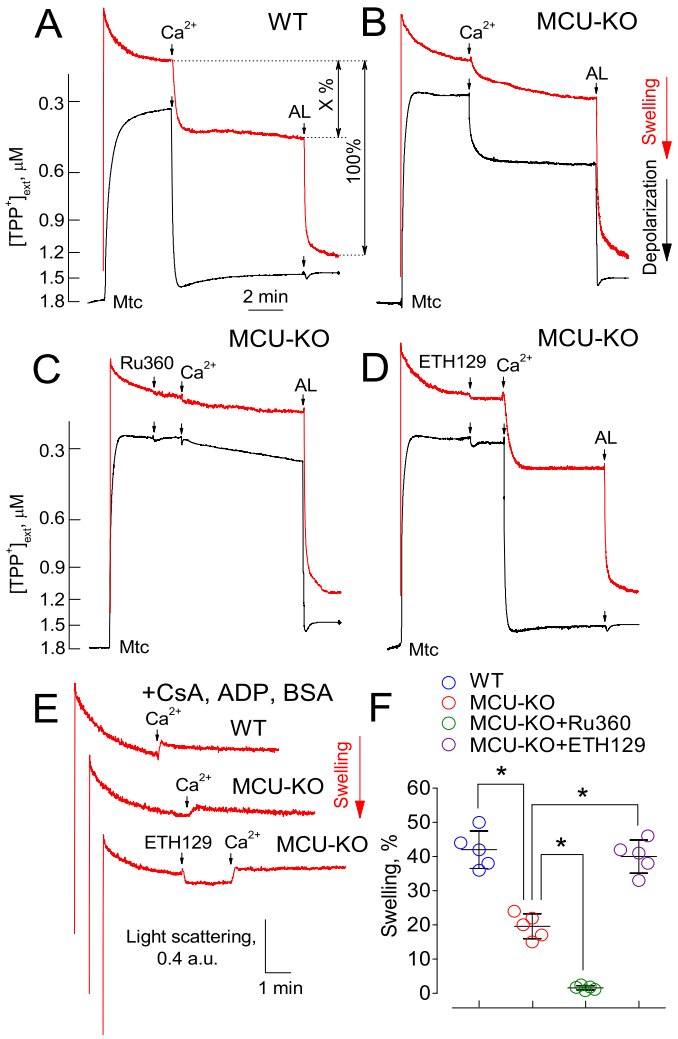

Figure 7. PTP induction in brain nonsynaptic mitochondria from WT and MCU-KO mice: ETH129 stimulates whereas Ru360 prevents Ca^{2+}-dependent PTP induction in MCU-KO mitochondria. *A–D*, light scattering (*red traces*), indicative of mitochondrial swelling, and TPP^+ concentration in the incubation medium (*black traces*), indicative of mitochondrial membrane potential, in experiments with WT (*A*) and MCU-KO (*B–D*) brain mitochondria fueled with 3 mM pyruvate plus 1 mM malate. An induction of the PTP was triggered by a 100 μM $CaCl_2$ pulse. Where indicated, 30 μg/ml alamethicin (*AL*) was added to induce maximal mitochondrial swelling. *C*, 3.3 μM Ru360 was added as indicated. *D*, 5 μM ETH129 was added as indicated. The *time bar* shown in *A* is applicable to *B*, *C*, and *D*. *E*, inhibition of PTP induction with PTP inhibitors. Where indicated, mitochondria fueled with 3 mM pyruvate plus 1 mM malate were treated with 100 μM $CaCl_2$, 5 μM ETH129, and a combination of PTP inhibitors: 1 μM CsA, 100 μM ADP (with 1 μM oligomycin), and 0.1% BSA (free from fatty acids). *F*, statistical analysis of mitochondrial swelling recorded 8 min after Ca^{2+} pulse and quantified as shown in *A*. Data are shown as mean ± S.D. (*error bars*), $n = 5$. *, $p < 0.001$ comparing the amount of swelling in MCU-KO mitochondria with either WT mitochondria, ETH129-treated MCU-KO mitochondria, or Ru360-treated MCU-KO mitochondria.

chondria at the end of experiments to produce maximal swelling. With MCU-KO nonsynaptic mitochondria, Ca^{2+} produced less swelling and depolarization compared with WT mitochondria, suggesting suppressed PTP induction (Fig. 7*B*). Ru360, an inhibitor of the Ca^{2+} uniporter (36), strongly inhibited PTP induction in MCU-KO mitochondria (Fig. 7*C*), consistent with strong inhibition of Ca^{2+} uptake in these mitochondria produced by this agent (Fig. 3*C*). ETH129, an electrophoretic Ca^{2+} ionophore (34) that accelerated Ca^{2+} influx into MCU-KO mitochondria (Fig. 3*C*), restored Ca^{2+}-

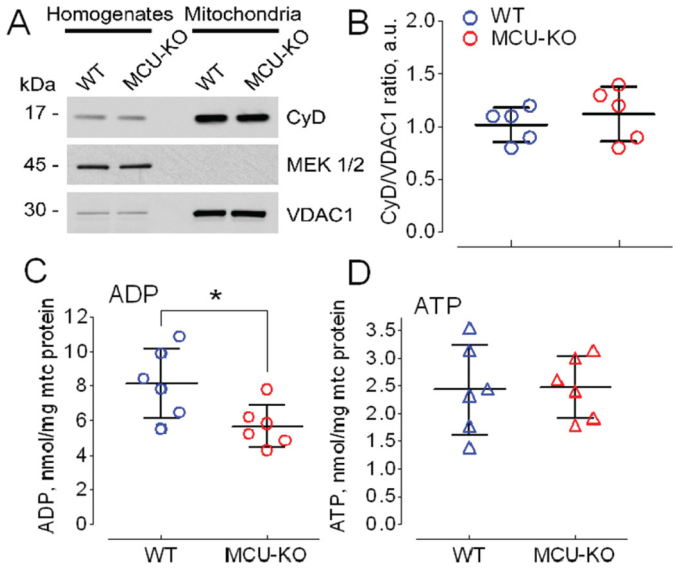

Figure 8. CyD expression and ADP and ATP content in brain nonsynaptic mitochondria isolated from WT and MCU-KO mice. *A*, Western blots demonstrating CyD levels in brain homogenates and nonsynaptic mitochondria isolated from brains of WT and MCU-KO mice. Note that despite the same protein loading for mitochondria and homogenate samples, there is enrichment of CyD and VDAC1 in the isolated mitochondria fraction compared with brain homogenates. MEK1/2 was used as a cytosolic marker to illustrate the purity of the mitochondrial preparation. VDAC1 was used as a loading control. *B*, statistical analysis of immunoblotting. Data represent a ratio of CyD to VDAC1 band intensities and are shown as mean ± S.D. (*error bars*) ($n = 5$). For ADP and ATP measurements (*C* and *D*, respectively), nonsynaptic mitochondria were incubated in the standard incubation medium supplemented with 3 mM pyruvate and 1 mM malate for 10 min at 37 °C. Then ADP and ATP levels were measured as described under "Experimental procedures." Data are shown as mean ± S.D. (*error bars*), $n = 6$. *, $p < 0.05$ comparing ADP content in WT *versus* MCU-KO mitochondria. *a.u.*, arbitrary units.

induced mitochondrial swelling and depolarization (Fig. 7*D*). To attribute mitochondrial swelling to PTP induction, we applied a combination of cyclosporin A (CsA), ADP, and BSA, known inhibitors of the PTP (Fig. 7*E*). The PTP inhibitors completely prevented Ca^{2+}-induced mitochondrial swelling, thus showing that it is attributable to PTP induction. Fig. 7*F* shows statistical analysis of these experiments. Overall, the presented data indicate that PTP induction in MCU-KO mitochondria is significantly but incompletely suppressed.

The expression of mitochondrial cyclophilin D (CyD) and the levels of ADP and ATP in mitochondria are major factors that regulate PTP induction (47). CyD sensitizes mitochondria to Ca^{2+}-triggered PTP induction (48, 49). Di- and triphosphate adenine nucleotides antagonize PTP induction by an incompletely understood mechanism (50). We assessed the CyD level in brain nonsynaptic mitochondria isolated from WT and MCU-KO mice and did not find a difference (Fig. 8). In parallel experiments, we assessed the levels of ADP and ATP in WT and MCU-KO brain nonsynaptic mitochondria (Fig. 8). ADP and ATP levels were comparable with those we reported previously (51). The difference in ATP levels was statistically insignificant, whereas ADP was slightly but statistically significantly decreased in mitochondria from MCU-KO mice. The reason for this difference is not clear. These data indicate that suppressed PTP induction in MCU-KO mitochondria was not due to a decrease in CyD expression or elevated ADP and/or ATP levels in these mitochondria.

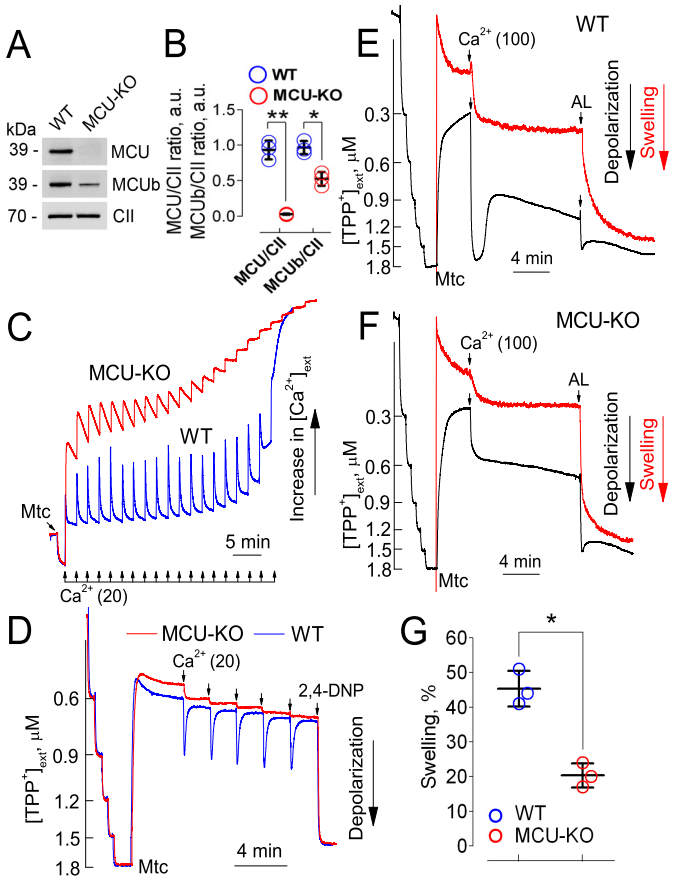

Figure 9. Ca^{2+} uptake, membrane potential, and PTP induction in brain synaptic mitochondria from MCU-KO and WT CD1 mice. *A*, Western blotting demonstrating the lack of MCU in brain synaptic mitochondria from MCU-KO mice and the presence of MCUb in mitochondria of WT and MCU-KO animals. A 70-kDa subunit of Complex II (*CII*) was used as a loading control. *B*, statistical analysis of immunoblotting. Data are mean ± S.D. (*error bars*) ($n = 3$). *, $p < 0.05$ comparing MCUb/Complex II in WT and MCU-KO mitochondria; **, $p < 0.001$ comparing MCU/Complex II in WT and MCU-KO mitochondria. *C*, Ca^{2+} uptake by brain synaptic mitochondria from WT (*blue trace*) and MCU-KO (*red trace*) mice. Here and in *D*, mitochondria (0.18 mg of protein/ml) were incubated in the standard incubation medium supplemented with 3 mM pyruvate plus 1 mM malate, 0.1 mM ADP, 1 μM oligomycin, and 0.1% BSA (free from fatty acids). *D*, effect of Ca^{2+} on mitochondrial membrane potential in WT (*blue trace*) and MCU-KO (*red trace*) synaptic mitochondria, respectively. In these experiments, 60 μM 2,4-DNP was used to depolarize mitochondria. *E* and *F*, light scattering (*red traces*), indicative of mitochondrial swelling, and TPP^+ concentration in the incubation medium (*black traces*), indicative of mitochondrial membrane potential, in experiments with WT (*E*) and MCU-KO (*F*) brain synaptic mitochondria fueled with 3 mM pyruvate plus 1 mM malate. *E* and *F*, mitochondria were incubated in the standard incubation medium without ADP, oligomycin, and BSA. An induction of the PTP was triggered by a 100 μM $CaCl_2$ pulse. Where indicated, 30 μg/ml alamethicin (*AL*) was added to induce maximal mitochondrial swelling. *G*, statistical analysis of mitochondrial swelling recorded 8 min after Ca^{2+} pulse. Data are mean ± S.D. (*error bars*), $n = 3$. *, $p < 0.01$ comparing the amount of swelling in WT and MCU-KO mitochondria. *a.u.*, arbitrary units.

Brain nonsynaptic mitochondria used in our study originated from neuronal somata and glial cells, whereas synaptic mitochondria are from nerve terminals and are of purely neuronal origin. We tested synaptic mitochondria from MCU-KO mice and found properties similar to nonsynaptic mitochondria (Fig. 9). The level of MCU in synaptic mitochondria from MCU-KO mice was below the detection limit of Western blotting (Fig. 9*A*). The level of MCUb in synaptic mitochondria from MCU-KO mice was 2-fold lower than in synaptic mitochondria from WT mice (Fig. 9, *A* and *B*). In synaptic mitochondria, deletion of MCU decreased the rate of Ca^{2+} uptake but did not completely prevent Ca^{2+} influx and membrane depolarization (Fig. 9, *C* and *D*). Consistent with this, MCU deletion in synaptic mitochondria inhibited Ca^{2+}-dependent PTP induction but failed to completely prevent it (Fig. 9, *E*–*G*).

Discussion

In the present study, we discovered a unique MCU-independent Ca^{2+} uptake mechanism existing in brain mitochondria isolated from MCU-KO mice (Figs. 1 and 9). We found that deletion of MCU significantly slows the rate of Ca^{2+} influx into brain mitochondria, but does not completely abolish it. Consistently, the Ca^{2+}-triggered induction of PTP in brain mitochondria from MCU-KO mice is hindered, but not completely prevented. Based on these findings, deletion of MCU may have limited ability to protect brain mitochondria from PTP induction and may incompletely protect neurons against glutamate-induced Ca^{2+} dysregulation and excitotoxicity, in which an induction of PTP in mitochondria plays a key role (52).

Ca^{2+} uptake by mitochondria plays an important role in regulation of cellular and mitochondrial functions. Mitochondria can accumulate large amounts of Ca^{2+}, contributing to maintenance of low resting cytosolic Ca^{2+} (9). In the mitochondrial matrix, Ca^{2+} can activate pyruvate, α-ketoglutarate, and isocitrate dehydrogenases, thereby stimulating mitochondrial respiration and oxidative phosphorylation (4). In our study, however, MCU deletion failed to cause significant changes in mitochondrial respiration, suggesting that this kind of regulation might be not essential. This is in line with the notion that rapid Ca^{2+} influx into mitochondria mediated by MCU does not regulate resting mitochondrial Ca^{2+} levels and, consequently, MCU does not affect the resting mitochondrial respiration. On the other hand, the excessive accumulation of Ca^{2+} in mitochondria may lead to the induction of PTP, manifested in mitochondrial depolarization and swelling (8). Both events were evaluated in our study, and both were significantly reduced in MCU-KO mitochondria compared with WT mitochondria.

The Ca^{2+}-induced PTP damages mitochondria and, therefore, is inextricably involved in mitochondrial pathophysiology. The molecular identity of PTP is still a matter of debate (53). However, it is well established that Ca^{2+} must enter mitochondria to induce the PTP (28). The Ca^{2+} uniporter is the main pathway for Ca^{2+} influx into mitochondria (10). Recently, the molecular identity of the Ca^{2+} uniporter was revealed (11, 12). It appears that the Ca^{2+} uniporter is composed of several subunits, among which MCU serves as the Ca^{2+} channel spanning the IMM (9). Consequently, genetic ablation of MCU in MCU-KO mice led to complete inhibition of Ca^{2+} uptake in skeletal muscle and heart mitochondria (22). How MCU deletion affects Ca^{2+} transport in brain mitochondria was not completely clear. Recently, Nichols *et al.* (54) reported that Ca^{2+} influx in brain mitochondria from MCU-KO mice was inhibited and PTP induction was hindered. However, in this study, mitochondrial depolarization induced by Ca^{2+} was not unequivocally attributed to PTP induction by preventing it with PTP inhibitors. In addition, it was not unambiguously proven

that inhibition of mitochondrial Ca^{2+} uptake is indeed due to MCU deletion. Whether putative inhibition of PTP induction was the result of suppressed Ca^{2+} influx into mitochondria or due to other factors remained unclear.

The lack of difference in CyD expression and comparable or higher levels of ADP and ATP in WT mitochondria are inconsistent with the idea that these factors might contribute to the decreased PTP induction in MCU-KO mitochondria. On the other hand, restoration of PTP induction in MCU-KO mitochondria in the presence of ETH129, an electrophoretic Ca^{2+} ionophore that can deliver Ca^{2+} into mitochondria (34, 35) and accelerate Ca^{2+} influx into MCU-KO mitochondria (Fig. 3*C*), suggests that inhibition of Ca^{2+} uptake due to MCU deletion is the main cause of PTP inhibition in MCU-KO mitochondria. Nevertheless, the residual Ca^{2+} uptake in MCU-KO mitochondria apparently could induce PTP in the fraction of vulnerable mitochondria. This explains why Ca^{2+} could inhibit respiration of MCU-KO mitochondria fueled by Complex I substrates. Under these conditions, recovery of mitochondrial respiration with succinate is consistent with previously published results (44). Further improvement with Cyt *c* and NADH suggests the loss of Cyt *c* and depletion of mitochondrial NADH due to PTP induction (44, 45) as the main mechanisms for respiratory inhibition.

The main unanswered question in our study concerns the mechanism of residual Ca^{2+} uptake in MCU-KO mitochondria. Previously, it was reported that mitochondria may possess an mRR that may contribute to mitochondrial Ca^{2+} uptake (39, 40). In addition, it has been well established that mitochondria possess a Na^+/Ca^{2+} exchanger (mNCX) responsible for Ca^{2+} efflux from mitochondria (55). It is possible that mNCX, similarly to plasmalemmal NCX (56, 57), may work in reverse under conditions of metabolic inhibition and/or elevated cytosolic Ca^{2+}, bringing Ca^{2+} into mitochondria (37, 38). To test these possibilities, we used dantrolene, an inhibitor of ryanodine receptor, previously used in experiments with mitochondria (39, 40), and CGP37157, an inhibitor of mNCX (41). We used these agents in concentrations that previously produced inhibitory effects on the corresponding targets, mRR or mNCX. In our experiments, however, neither of these agents affected the residual Ca^{2+} uptake by MCU-KO mitochondria. On the other hand, Ru360, an inhibitor of the Ca^{2+} uniporter (36), completely blocked Ca^{2+} uptake by MCU-KO mitochondria. The question remains as to which protein(s) interacts with Ru360 in the absence of MCU and how this leads to complete inhibition of residual Ca^{2+} uptake.

It is possible that mitochondria possess MCU-independent pathways for Ca^{2+} uptake (58, 59). One of the possible candidates for the MCU-independent Ca^{2+} uptake pathways is MCUb (14), which was detected in isolated brain mitochondria (Figs. 1*B* and 9*A*). Although Raffaello *et al.* (14) proposed that MCUb forms a nonconducting channel and this correlated with the lack of Glu-257 in MCUb, the structure study by Oxenoid *et al.* (60) argued against that conclusion. They found that the Glu-257 is dispensable for Ca^{2+} uptake, thus implying that MCUb could also conduct Ca^{2+}. In addition, it is known that Ser-259 of MCU is responsible for inhibition of the MCU-mediated Ca^{2+} uptake by Ru360 (12, 60). This Ser-259 is conserved both in MCU and MCUb. These previous studies therefore raised the possibility that MCUb could be responsible for the MCU KO–resistant and Ru360-sensitive mitochondrial Ca^{2+} uptake found in the present study. Alternatively, our data obtained with brain mitochondria do not rule out the possibility that MCU might not be a Ca^{2+} channel, but instead could be an accessory, regulatory subunit of the mitochondrial Ca^{2+} transport complex. However, our experiments with liver, heart, and skeletal muscle mitochondria as well as experiments with MCU reconstituted in the planar lipid bilayer, in which MCU ion channel activity has been detected (11), argue against these hypotheses.

Interestingly, a low expression of MCU and high expression of MCUb in WT heart mitochondria correlated with high Ca^{2+} uptake capacity of heart mitochondria compared with liver and skeletal muscle mitochondria. The amount of Ca^{2+} that can be accumulated by mitochondria is limited due to PTP induction (30). Consequently, our findings suggest that the levels of expression of MCU and MCUb may determine the propensity to PTP induction in mitochondria.

The failure to completely block Ca^{2+} uptake by genetic ablation of MCU in brain mitochondria and, subsequently, incomplete prevention of PTP induction suggests that targeting MCU alone might not be very efficacious in protecting neurons from glutamate-induced Ca^{2+} dysregulation and glutamate excitotoxicity. It is conceivable that combined deletion of MCU and CyD might be much more effective in neuroprotection. CyD deletion increases mitochondrial Ca^{2+} uptake capacity, inhibits PTP induction, and augments resistance of neurons to deleterious effect of glutamate (52). However, this neuroprotection is limited. An exposure to higher glutamate concentrations that cause larger Ca^{2+} influx in the cell and, subsequently, into mitochondria, may overcome neuroprotection achieved by CyD deletion (52). It would be very interesting to test in future studies whether a combination of CyD and MCU deletions would result in stronger neuroprotection and whether simultaneous pharmacological inhibition of CyD and MCU could be a valid approach in protecting brain cells from insults associated with elevation of Ca^{2+} influx into neurons.

Experimental procedures

Materials

Pyruvate, malate, succinate, glutamate, EGTA, ADP, oligomycin, 2,4-dinitrophenol, CGP37157, ETH129, dantrolene, and carbonyl cyanide *p*-trifluoromethoxyphenylhydrazone (FCCP), rat Cyt *c*, and NADH were purchased from Sigma. Tetraphenylphosphonium chloride was from Fluka (Buchs, Switzerland). Percoll was from GE Healthcare. Ru360 was from Calbiochem. BSA, free from free fatty acids, was from MP Biomedicals (Irvine, CA). Alamethicin was from Enzo (Farmingdale, NY).

Animals

All procedures with animals were performed in accordance with the institutional animal care and use committee–approved protocol. The breeders of MCU-KO mice were obtained from Dr. Toren Finkel (Center for Molecular Medicine, NHLBI, National Institutes of Health), and breeding col-

onies were established in the Laboratory Animal Resource Center at Indiana University School of Medicine (Indianapolis, IN). The mice were maintained on a CD1 (Charles River Laboratories, Wilmington, MA) background, and experimental homozygous mice were obtained by heterozygous crosses (22). Age- and sex-matched WT littermates were used as controls. The mice were housed under standard conditions with free access to water and food. In our experiments, we used animals of both sexes. However, in every individual experiment, we only used animals of the same sex. We did not find any significant difference in the results obtained with either sex, and therefore, the data were pooled together for statistical analysis.

Genotyping

All offspring were genotyped using a PCR assay on tail DNA with the forward primer: GT F2 (5′-GGAGTTAAGTCATGAGCTGCTAT-3′) and reverse primers GT R2 (5′-CTGGCTTAGTTGGCAGAGTTC-3′) and V76R (5′-CCAATAAACCCTCTTGCAGTTGC-3′) (22) and the Platinum PCR Super Mix (Invitrogen) for amplification. The PCR conditions were as follows: initial denaturation at 94 °C for 2 min, followed by 35 cycles (94 °C for 30 s, 60 °C for 30 s, and 72 °C for 30 s) and then 5 min at 72 °C. Reaction products were analyzed on 1.2% agarose gel run at 100 V for 60 min with Tris acetate–EDTA running buffer containing 1× GelRed™ nucleic acid gel stain (Biotium, Fremont, CA).

Isolation of brain, liver, heart, and skeletal muscle mitochondria

Percoll gradient–purified brain nonsynaptic and synaptic mitochondria from homozygous MCU-KO mice and WT littermates were isolated as we described previously (61). Briefly, brains from three mice of each strain were harvested and processed simultaneously. Following brain tissue homogenization in a 15-ml glass Dounce homogenizer (10 strokes with pestle A, 30 strokes with pestle B) on ice, homogenates were diluted with 30 ml of Isolation Buffer 1 and centrifuged for 10 min at 2,400 rpm in the Beckman centrifuge Avanti J-26XP, rotor JA-25.50 (700 × *g*). This and all other procedures and centrifugations were performed at 0–2 °C. Then supernatant was centrifuged for 10 min at 12,500 rpm (18,900 × *g*) in the Beckman centrifuge Avanti J-26XP, rotor JA-25.50. Supernatant was discarded, and the pellet was resuspended in 35 ml of Isolation Buffer 2 and centrifuged for 10 min at 12,500 rpm (18,850 × *g*) in the Beckman centrifuge Avanti J-26XP, rotor JA-25.50. Next, the pellet was resuspended in 5 ml of Isolation Buffer 3. The suspension was layered onto the top of the Percoll gradient (26%/40%) in Beckman Ultra-Clear centrifuge tubes and centrifuged for 28 min at 15,500 rpm (41,100 × *g*) in the Beckman ultracentrifuge Optima L100K, bucket rotor SW41Ti. Nonsynaptic mitochondria were resuspended in Isolation Buffer 3 and centrifuged for 20 min at 15,500 rpm (41,100 × *g*) in the Beckman ultracentrifuge Optima L100K, bucket rotor SW41Ti. The pellet was resuspended in Isolation Buffer 3 and centrifuged again for 20 min at 15,500 rpm (41,100 × *g*) in the Beckman ultracentrifuge Optima L100K, bucket rotor SW41Ti. The pellet of nonsynaptic mitochondria was collected, resuspended in 0.15 ml of Isolation Buffer 3, and stored on ice. Isolation Buffer 1 contained 225 mM mannitol, 75 mM sucrose, 10 mM Hepes, pH 7.4, adjusted with KOH, 0.1% BSA, free from fatty acids, and 1 mM EGTA. Isolation Buffer 2 contained 225 mM mannitol, 75 mM sucrose, 10 mM Hepes, pH 7.4, adjusted with KOH, 0.1 mM EGTA. Isolation Buffer 3 contained 395 mM sucrose, 0.1 mM EGTA, 10 mM Hepes, pH 7.4. 26% Percoll in Percoll Buffer was prepared with 5.2 ml of Percoll (Sigma) and 14.8 ml of Percoll Buffer; 40% Percoll in Percoll Buffer was prepared with 8 ml of Percoll and 12 ml of Percoll Buffer. Percoll Buffer contained 320 mM sucrose, 1 mM EGTA, 10 mM Hepes, pH 7.4.

Synaptic mitochondria were isolated from synaptosomes by the nitrogen cavitation method using a nitrogen cell disruption bomb, model 4639 (Parr Instrument Co., Moline, IL), cooled on ice (42) with some modifications. Briefly, the synaptosomes obtained during preparation of nonsynaptic mitochondria were transferred to a cooled beaker and placed into the nitrogen bomb on ice under 1,100 p.s.i. for 13 min. Then synaptosomes were layered on top of the discontinuous Percoll gradient (24%/40%) and centrifuged at 15,500 rpm (41,100 × *g*) for 28 min in a ultracentrifuge Optima L100K, bucket rotor SW41Ti. The mitochondrial fraction in the interface between Percoll layers was transferred into a fresh tube; diluted 1:5 with medium containing 395 mM sucrose, 0.1 mM EGTA, 10 mM Hepes, pH 7.4; and centrifuged for 20 min at 15,500 rpm (41,100 × *g*) in the Beckman ultracentrifuge Optima L100K, bucket rotor SW41Ti. The pellet was resuspended in 0.15 ml of the latter medium and kept on ice.

Liver, heart, and skeletal muscle mitochondria were isolated and purified in the same way as nonsynaptic brain mitochondria, but without Percoll gradient purification. Liver tissue from one mouse per strain was homogenized using 30 ml of Potter–Elvehjem homogenizers, and then mitochondria were isolated using differential centrifugation as described for nonsynaptic mitochondria before Percoll gradient purification. Hearts from three mice per strain as well as skeletal muscle (quadriceps of one hind limb) from one mouse per strain were disintegrated using Tissue Master 125 grinder (OMNI International, Kennesaw, GA). Then tissues were homogenized using 30-ml Potter–Elvehjem homogenizers, and mitochondria were isolated using differential centrifugation as described for nonsynaptic mitochondria without Percoll gradient purification. Mitochondrial protein concentration was measured by the Bradford method (44) with BSA as a standard.

Mitochondrial Ca^{2+} uptake measurements

Mitochondrial Ca^{2+} uptake was measured with a miniature Ca^{2+}-selective electrode in a 0.3-ml chamber at 37 °C under continuous stirring. A decrease in Ca^{2+} concentration in the incubation medium indicated mitochondrial Ca^{2+} uptake. Here and in other experiments with isolated mitochondria, the standard incubation medium contained 125 mM KCl, 0.5 mM $MgCl_2$, 3 mM KH_2PO_4, 10 mM Hepes, pH 7.4, 10 μM EGTA and was supplemented with 3 mM pyruvate plus 1 mM malate. In addition, in some experiments, the incubation medium was supplemented with 0.1 mM ADP and 1 μM oligomycin as described previously (30) and with 0.1% BSA (free from fatty acids, MP Biochemicals, Santa Ana, CA) as indicated. Ca^{2+} was delivered to mitochondria as 10, 20, or 100 μM $CaCl_2$ pulses.

Ca^{2+} uptake rates were quantified as nmol of Ca^{2+}/min/mg of mitochondrial protein.

Mitochondrial respiration

Mitochondrial respiration was assessed in a 0.4-ml continuously stirred chamber containing the standard incubation medium, which was supplemented either with 3 mM pyruvate plus 1 mM malate or 3 mM succinate plus 3 mM glutamate. In experiments with succinate, glutamate was used to prevent inhibition of succinate dehydrogenase by oxaloacetate due to elimination of oxaloacetate in the reaction catalyzed by aspartate aminotransferase (43, 62). The chamber was maintained at 37 °C and was equipped with a Clark-type oxygen electrode and a tightly sealed lid. The slope of the oxygen consumption trace corresponded to the respiratory rate.

Mitochondrial swelling and membrane potential

Mitochondrial swelling was evaluated in a 0.3-ml continuously stirred chamber at 37 °C by following changes in light scattering of mitochondrial suspension at 525 nm with an incident light beam at 180° relative to the photodetector. The incubation medium for light scattering measurements contained 215 mM mannitol, 70 mM sucrose, 0.5 mM $MgCl_2$, 3 mM KH_2PO_4, 10 mM Hepes, pH 7.4, 10 μM EGTA, 3 mM pyruvate, 1 mM malate. A decrease in light scattering of mitochondrial suspension indicated mitochondrial swelling. Maximal mitochondrial swelling was induced by alamethicin (30 μg/ml), which was considered as 100% swelling. Ca^{2+}-induced swelling was calculated as a percentage of maximal, alamethicin-induced swelling (63). Mitochondrial membrane potential was assessed simultaneously with mitochondrial swelling with a TPP^+ electrode by monitoring TPP^+ distribution between the incubation medium and mitochondria (64). A decrease in external TPP^+ concentration corresponds to mitochondrial polarization, whereas an increase of TPP^+ concentration in the incubation medium corresponds to depolarization.

Immunoblotting

Brain isolated mitochondria pretreated with Protease Inhibitor Mixture (Roche Diagnostics) were solubilized by incubation in NuPAGE LDS sample buffer (Invitrogen) supplemented with a reducing agent at 70 °C for 15 min. BisTris Mops gels (12%; Invitrogen) were used for electrophoresis (10 μg of protein/lane). After electrophoresis, proteins were transferred to Hybond-ECL nitrocellulose membrane (Amersham Biosciences). Blots were incubated for 1 h at room temperature in blocking solution of 5% BSA, PBS, pH 7.2, and 0.15% Triton X-100. Then blots were incubated with one of the following primary antibodies: mouse monoclonal anti-Complex II 70-kDa subunit (Invitrogen; 1:1000), mouse monoclonal anti-cyclophilin D antibody (Calbiochem; 1:500), and rabbit polyclonal anti-VDAC1 (Calbiochem; 1:1000), rabbit monoclonal anti-MEK1/2 (Pierce; 1:1000). For detection of MCU, we used a rabbit polyclonal antibody (Atlas Antibodies (Bromma, Sweden), catalog no. HPA016480; 1:1,000) previously used by other investigators (22, 65, 66). For detection of MCUb, we used goat polyclonal antibody (Santa Cruz Biotechnology, Inc. (Dallas, TX), catalog no. sc-163985; 1:250). Blots were incubated with goat anti-mouse or goat anti-rabbit IgG (1:20,000) coupled with horseradish peroxidase (Jackson ImmunoResearch Laboratories, West Grove, PA) and developed with Supersignal West Pico chemiluminescent reagents (Pierce). Molecular mass markers See Blue Plus 2 Standards (5 μl) and HiMark prestained high-molecular weight protein standards (10 μl) (Invitrogen) were used to determine molecular masses of the bands. NIH ImageJ version 1.48 (National Institutes of Health) was used to quantify band densities.

Mitochondrial ADP and ATP content

ADP and ATP levels were determined using a luciferin/luciferase-based ATP bioluminescent somatic cell assay kit (Sigma) and a GloMax 20/20 luminometer (Promega, Madison, WI). Mitochondria were incubated for 10 min at 37 °C in the standard incubation medium supplemented with 3 mM pyruvate plus 1 mM malate, and then ADP and ATP were measured. Measurements were made in 4% perchloric acid extracts neutralized by KOH following the kit manufacturer's suggestions. ADP was converted to ATP using pyruvate kinase in the presence of phosphoenolpyruvate (67).

Statistics

Data are shown as mean ± S.D. of the indicated number of separate experiments. Statistical analysis of the experimental results consisted of unpaired *t* test or one-way analysis of variance followed by Bonferroni's post hoc test if applicable (GraphPad Prism® version 4.0, GraphPad Software Inc., La Jolla, CA). Every experiment was performed using several different preparations of isolated mitochondria.

Author contributions—J. H. conducted most of the experiments, analyzed the results, and contributed to writing the paper. T. B. maintained the MCU-KO breeding colony, conducted genotyping and immunoblotting experiments, and analyzed the results. J. E. R. and Z. L. maintained the MCU-KO colony and conducted genotyping. Y. M. U. analyzed the results and contributed to writing the paper. N. B. conceived the idea for the project, analyzed the results, and wrote the paper. All authors reviewed the results and approved the final version of the manuscript.

Acknowledgment—We thank Dr. Toren Finkel for providing a breeding pair of MCU-KO mice.

References

1. Deluca, H. F., and Engstrom, G. W. (1961) Calcium uptake by rat kidney mitochondria. *Proc. Natl. Acad. Sci. U.S.A.* **47,** 1744–1750 CrossRef Medline
2. Vasington, F. D., and Murphy, J. V. (1962) Ca ion uptake by rat kidney mitochondria and its dependence on respiration and phosphorylation. *J. Biol. Chem.* **237,** 2670–2677 Medline
3. Zoratti, M., and Szabò, I. (1995) The mitochondrial permeability transition. *Biochim. Biophys. Acta* **1241,** 139–176 CrossRef Medline
4. Denton, R. M. (2009) Regulation of mitochondrial dehydrogenases by calcium ions. *Biochim. Biophys. Acta* **1787,** 1309–1316 CrossRef Medline
5. Kiedrowski, L., and Costa, E. (1995) Glutamate-induced destabilization of intracellular calcium concentration homeostasis in cultured cerebellar granule cells: role of mitochondria in calcium buffering. *Mol. Pharmacol.* **47,** 140–147 Medline

6. White, R. J., and Reynolds, I. J. (1995) Mitochondria and Na^+/Ca^{2+} exchange buffer glutamate-induced calcium loads in cultured cortical neurons. *J. Neurosci.* **15,** 1318–1328 CrossRef Medline
7. Wang, G. J., and Thayer, S. A. (1996) Sequestration of glutamate-induced Ca^{2+} loads by mitochondria in cultured rat hippocampal neurons. *J. Neurophysiol.* **76,** 1611–1621 CrossRef Medline
8. Bernardi, P. (1999) Mitochondrial transport of cations: channels, exchangers, and permeability transition. *Physiol. Rev.* **79,** 1127–1155 CrossRef Medline
9. Foskett, J. K., and Philipson, B. (2015) The mitochondrial Ca^{2+} uniporter complex. *J. Mol. Cell Cardiol.* **78,** 3–8 CrossRef Medline
10. De Stefani, D., Patron, M., and Rizzuto, R. (2015) Structure and function of the mitochondrial calcium uniporter complex. *Biochim. Biophys. Acta* **1853,** 2006–2011 CrossRef Medline
11. De Stefani, D., Raffaello, A., Teardo, E., Szabò, I., and Rizzuto, R. (2011) A forty-kilodalton protein of the inner membrane is the mitochondrial calcium uniporter. *Nature* **476,** 336–340 CrossRef Medline
12. Baughman, J. M., Perocchi, F., Girgis, H. S., Plovanich, M., Belcher-Timme, C. A., Sancak, Y., Bao, X. R., Strittmatter, L., Goldberger, O., Bogorad, R. L., Koteliansky, V., and Mootha, V. K. (2011) Integrative genomics identifies MCU as an essential component of the mitochondrial calcium uniporter. *Nature* **476,** 341–345 CrossRef Medline
13. Chaudhuri, D., Sancak, Y., Mootha, V. K., and Clapham, D. E. (2013) MCU encodes the pore conducting mitochondrial calcium currents. *Elife* **2,** e00704 Medline
14. Raffaello, A., De Stefani, D., Sabbadin, D., Teardo, E., Merli, G., Picard, A., Checchetto, V., Moro, S., Szabò, I., and Rizzuto, R. (2013) The mitochondrial calcium uniporter is a multimer that can include a dominant-negative pore-forming subunit. *EMBO J.* **32,** 2362–2376 CrossRef Medline
15. Patron, M., Checchetto, V., Raffaello, A., Teardo, E., Vecellio Reane, D., Mantoan, M., Granatiero, V., Szabò, I., De Stefani, D., and Rizzuto, R. (2014) MICU1 and MICU2 finely tune the mitochondrial Ca^{2+} uniporter by exerting opposite effects on MCU activity. *Mol. Cell* **53,** 726–737 CrossRef Medline
16. Plovanich, M., Bogorad, R. L., Sancak, Y., Kamer, K. J., Strittmatter, L., Li, A. A., Girgis, H. S., Kuchimanchi, S., De Groot, J., Speciner, L., Taneja, N., Oshea, J., Koteliansky, V., and Mootha, V. K. (2013) MICU2, a paralog of MICU1, resides within the mitochondrial uniporter complex to regulate calcium handling. *PLoS One* **8,** e55785 CrossRef Medline
17. Csordás, G., Golenár, T., Seifert, E. L., Kamer, K. J., Sancak, Y., Perocchi, F., Moffat, C., Weaver, D., de la Fuente Perez, S., Bogorad, R., Koteliansky, V., Adijanto, J., Mootha, V. K., and Hajnóczky, G. (2013) MICU1 controls both the threshold and cooperative activation of the mitochondrial Ca^{2+} uniporter. *Cell Metab.* **17,** 976–987 CrossRef Medline
18. Sancak, Y., Markhard, A. L., Kitami, T., Kovács-Bogdán, E., Kamer, K. J., Udeshi, N. D., Carr, S. A., Chaudhuri, D., Clapham, D. E., Li, A. A., Calvo, S. E., Goldberger, O., and Mootha, V. K. (2013) EMRE is an essential component of the mitochondrial calcium uniporter complex. *Science* **342,** 1379–1382 CrossRef Medline
19. Mallilankaraman, K., Cárdenas, C., Doonan, P. J., Chandramoorthy, H. C., Irrinki, K. M., Golenár, T., Csordás, G., Madireddi, P., Yang, J., Müller, M., Miller, R., Kolesar, J. E., Molgó, J., Kaufman, B., Hajnóczky, G., *et al.* (2012) MCUR1 is an essential component of mitochondrial Ca^{2+} uptake that regulates cellular metabolism. *Nat. Cell Biol.* **14,** 1336–1343 CrossRef Medline
20. Moore, C. L. (1971) Specific inhibition of mitochondrial Ca^{++} transport by ruthenium red. *Biochem. Biophys. Res. Commun.* **42,** 298–305 CrossRef Medline
21. Vasington, F. D., Gazzotti, P., Tiozzo, R., and Carafoli, E. (1972) The effect of ruthenium red on Ca^{2+} transport and respiration in rat liver mitochondria. *Biochim. Biophys. Acta* **256,** 43–54 CrossRef Medline
22. Pan, X., Liu, J., Nguyen, T., Liu, C., Sun, J., Teng, Y., Fergusson, M. M., Rovira, I. I., Allen, M., Springer, D. A., Aponte, A. M., Gucek, M., Balaban, R. S., Murphy, E., and Finkel, T. (2013) The physiological role of mitochondrial calcium revealed by mice lacking the mitochondrial calcium uniporter. *Nat. Cell Biol.* **15,** 1464–1472 CrossRef Medline
23. Mnatsakanyan, N., Beutner, G., Porter, G. A., Alavian, K. N., and Jonas, E. A. (2017) Physiological roles of the mitochondrial permeability transition pore. *J. Bioenerg. Biomembr.* **49,** 13–25 CrossRef Medline
24. Izzo, V., Bravo-San Pedro, J. M., Sica, V., Kroemer, G., and Galluzzi, L. (2016) Mitochondrial permeability transition: new findings and persisting uncertainties. *Trends Cell Biol.* **26,** 655–667 CrossRef Medline
25. Schinder, A. F., Olson, E. C., Spitzer, N. C., and Montal, M. (1996) Mitochondrial dysfunction is a primary event in glutamate neurotoxicity. *J. Neurosci.* **16,** 6125–6133 CrossRef Medline
26. Nieminen, A. L., Petrie, T. G., Lemasters, J. J., and Selman, W. R. (1996) Cyclosporin A delays mitochondrial depolarization induced by *N*-methyl-D-aspartate in cortical neurons: evidence of the mitochondrial permeability transition. *Neuroscience* **75,** 993–997 CrossRef Medline
27. White, R. J., and Reynolds, I. J. (1996) Mitochondrial depolarization in glutamate-stimulated neurons: an early signal specific to excitotoxin exposure. *J. Neurosci.* **16,** 5688–5697 CrossRef Medline
28. Hunter, D. R., and Haworth, R. A. (1979) The Ca^{2+}-induced membrane transition in mitochondria. I. The protective mechanisms. *Arch. Biochem. Biophys.* **195,** 453–459 CrossRef Medline
29. Qiu, J., Tan, Y. W., Hagenston, A. M., Martel, M. A., Kneisel, N., Skehel, P. A., Wyllie, D. J., Bading, H., and Hardingham, G. E. (2013) Mitochondrial calcium uniporter Mcu controls excitotoxicity and is transcriptionally repressed by neuroprotective nuclear calcium signals. *Nat. Commun.* **4,** 2034 CrossRef Medline
30. Chalmers, S., and Nicholls, D. G. (2003) The relationship between free and total calcium concentrations in the matrix of liver and brain mitochondria. *J. Biol. Chem.* **278,** 19062–19070 CrossRef Medline
31. Spector, A. A., John, K., and Fletcher, J. E. (1969) Binding of long-chain fatty acids to bovine serum albumin. *J. Lipid Res.* **10,** 56–67 Medline
32. Di Paola, M., and Lorusso, M. (2006) Interaction of free fatty acids with mitochondria: coupling, uncoupling and permeability transition. *Biochim. Biophys. Acta* **1757,** 1330–1337 CrossRef Medline
33. Brustovetsky, N. (2016) Mitochondrial permeability transition: a look from a different angle. In *The Functions, Disease-related Dysfunctions, and Therapeutic Targeting of Neuronal Mitochondria* (Gribkoff, V. K., Jonas, E. A., and Hardwick, J. M., eds) p. 3–30, John Wiley & Sons, Inc., Hoboken, NJ
34. Prestipino, G., Falugi, C., Falchetto, R., and Gazzotti, P. (1993) The ionophore ETH 129 as Ca^{2+} translocator in artificial and natural membranes. *Anal. Biochem.* **210,** 119–122 CrossRef Medline
35. Jung, D. W., Bradshaw, P. C., Litsky, M., and Pfeiffer, D. R. (2004) Ca^{2+} transport in mitochondria from yeast expressing recombinant aequorin. *Anal. Biochem.* **324,** 258–268 CrossRef Medline
36. Ying, W. L., Emerson, J., Clarke, M. J., and Sanadi, D. R. (1991) Inhibition of mitochondrial calcium ion transport by an oxo-bridged dinuclear ruthenium ammine complex. *Biochemistry* **30,** 4949–4952 CrossRef Medline
37. Griffiths, E. J. (1999) Reversal of mitochondrial Na/Ca exchange during metabolic inhibition in rat cardiomyocytes. *FEBS Lett.* **453,** 400–404 CrossRef Medline
38. Smets, I., Caplanusi, A., Despa, S., Molnar, Z., Radu, M., VandeVen, M., Ameloot, M., and Steels, P. (2004) Ca^{2+} uptake in mitochondria occurs via the reverse action of the Na^+/Ca^{2+} exchanger in metabolically inhibited MDCK cells. *Am. J. Physiol. Renal Physiol.* **286,** F784–F794 CrossRef Medline
39. Beutner, G., Sharma, V. K., Giovannucci, D. R., Yule, D. I., and Sheu, S. S. (2001) Identification of a ryanodine receptor in rat heart mitochondria. *J. Biol. Chem.* **276,** 21482–21488 CrossRef Medline
40. Jakob, R., Beutner, G., Sharma, V. K., Duan, Y., Gross, R. A., Hurst, S., Jhun, B. S., O-Uchi, J., and Sheu, S. S. (2014) Molecular and functional identification of a mitochondrial ryanodine receptor in neurons. *Neurosci. Lett.* **575,** 7–12 CrossRef Medline
41. Cox, D. A., and Matlib, M. A. (1993) Modulation of intramitochondrial free Ca^{2+} concentration by antagonists of Na^+-Ca^{2+} exchange. *Trends Pharmacol. Sci.* **14,** 408–413 CrossRef Medline
42. Wojtczak, A. B. (1969) Inhibitory action of oxaloacetate on succinate oxidation in rat-liver mitochondria and the mechanism of its reversal. *Biochim. Biophys. Acta* **172,** 52–65 CrossRef Medline

43. Oestreicher, A. B., van den Bergh, S. G., and Slater, E. C. (1969) The inhibition by 2,4-dinitrophenol of the removal of oxaloacetate formed by the oxidation of succinate by rat-liver and -heart mitochondria. *Biochim. Biophys. Acta* **180,** 45–55 CrossRef Medline
44. Brustovetsky, N., Brustovetsky, T., Jemmerson, R., and Dubinsky, J. M. (2002) Calcium-induced cytochrome *c* release from CNS mitochondria is associated with the permeability transition and rupture of the outer membrane. *J. Neurochem.* **80,** 207–218 CrossRef Medline
45. Di Lisa, F., Menabò, R., Canton, M., Barile, M., and Bernardi, P. (2001) Opening of the mitochondrial permeability transition pore causes depletion of mitochondrial and cytosolic NAD^+ and is a causative event in the death of myocytes in postischemic reperfusion of the heart. *J. Biol. Chem.* **276,** 2571–2575 CrossRef Medline
46. Vodyanoy, I., Bezrukov, S. M., and Parsegian, V. A. (1993) Probing alamethicin channels with water-soluble polymers. Size-modulated osmotic action. *Biophys. J.* **65,** 2097–2105 CrossRef Medline
47. Rasola, A., and Bernardi, P. (2007) The mitochondrial permeability transition pore and its involvement in cell death and in disease pathogenesis. *Apoptosis* **12,** 815–833 CrossRef Medline
48. Brustovetsky, N., Brustovetsky, T., Purl, K. J., Capano, M., Crompton, M., and Dubinsky, J. M. (2003) Increased susceptibility of striatal mitochondria to calcium-induced permeability transition. *J. Neurosci.* **23,** 4858–4867 CrossRef Medline
49. Basso, E., Fante, L., Fowlkes, J., Petronilli, V., Forte, M. A., and Bernardi, P. (2005) Properties of the permeability transition pore in mitochondria devoid of Cyclophilin D. *J. Biol. Chem.* **280,** 18558–18561 CrossRef Medline
50. Novgorodov, S. A., Gudz, T. I., Milgrom, Y. M., and Brierley, G. P. (1992) The permeability transition in heart mitochondria is regulated synergistically by ADP and cyclosporin A. *J. Biol. Chem.* **267,** 16274–16282 Medline
51. Hamilton, J., Pellman, J. J., Brustovetsky, T., Harris, R. A., and Brustovetsky, N. (2015) Oxidative metabolism in YAC128 mouse model of Huntington's disease. *Hum. Mol. Genet.* **24,** 4862–4878 CrossRef Medline
52. Li, V., Brustovetsky, T., and Brustovetsky, N. (2009) Role of cyclophilin D-dependent mitochondrial permeability transition in glutamate-induced calcium deregulation and excitotoxic neuronal death. *Exp. Neurol.* **218,** 171–182 CrossRef Medline
53. Chinopoulos, C. (2018) Mitochondrial permeability transition pore: back to the drawing board. *Neurochem. Int.* **117,** 49–54 CrossRef Medline
54. Nichols, M., Elustondo, P. A., Warford, J., Thirumaran, A., Pavlov, E. V., and Robertson, G. S. (2017) Global ablation of the mitochondrial calcium uniporter increases glycolysis in cortical neurons subjected to energetic stressors. *J. Cereb. Blood Flow Metab.* **37,** 3027–3041 CrossRef Medline
55. Cox, D. A., and Matlib, M. A. (1993) A role for the mitochondrial Na^+-Ca^{2+} exchanger in the regulation of oxidative phosphorylation in isolated heart mitochondria. *J. Biol. Chem.* **268,** 938–947 Medline
56. Hoyt, K. R., Arden, S. R., Aizenman, E., and Reynolds, I. J. (1998) Reverse Na^+/Ca^{2+} exchange contributes to glutamate-induced intracellular Ca^{2+} concentration increases in cultured rat forebrain neurons. *Mol. Pharmacol.* **53,** 742–749 CrossRef Medline
57. Kiedrowski, L. (1999) *N*-Methyl-D-aspartate excitotoxicity: relationships among plasma membrane potential, Na^+/Ca^{2+} exchange, mitochondrial Ca^{2+} overload, and cytoplasmic concentrations of Ca^{2+}, H^+, and K^+. *Mol. Pharmacol.* **56,** 619–632 CrossRef Medline
58. Bondarenko, A. I., Jean-Quartier, C., Malli, R., and Graier, W. F. (2013) Characterization of distinct single-channel properties of Ca^{2+} inward currents in mitochondria. *Pflugers Arch.* **465,** 997–1010 CrossRef Medline
59. Bondarenko, A. I., Jean-Quartier, C., Parichatikanond, W., Alam, M. R., Waldeck-Weiermair, M., Malli, R., and Graier, W. F. (2014) Mitochondrial Ca^{2+} uniporter (MCU)-dependent and MCU-independent Ca^{2+} channels coexist in the inner mitochondrial membrane. *Pflugers Arch.* **466,** 1411–1420 CrossRef Medline
60. Oxenoid, K., Dong, Y., Cao, C., Cui, T., Sancak, Y., Markhard, A. L., Grabarek, Z., Kong, L., Liu, Z., Ouyang, B., Cong, Y., Mootha, V. K., and Chou, J. J. (2016) Architecture of the mitochondrial calcium uniporter. *Nature* **533,** 269–273 CrossRef Medline
61. Pellman, J. J., Hamilton, J., Brustovetsky, T., and Brustovetsky, N. (2015) Ca^{2+} handling in isolated brain mitochondria and cultured neurons derived from the YAC128 mouse model of Huntington's disease. *J. Neurochem.* **134,** 652–667 CrossRef Medline
62. Wojtczak, L., Wojtczak, A. B., and Ernster, L. (1969) The inhibition of succinate dehydrogenase by oxalacetate. *Biochim. Biophys. Acta* **191,** 10–21 CrossRef Medline
63. Li, T., Brustovetsky, T., Antonsson, B., and Brustovetsky, N. (2010) Dissimilar mechanisms of cytochrome *c* release induced by octyl glucoside-activated BAX and by BAX activated with truncated BID. *Biochim. Biophys. Acta* **1797,** 52–62 CrossRef Medline
64. Kamo, N., Muratsugu, M., Hongoh, R., and Kobatake, Y. (1979) Membrane potential of mitochondria measured with an electrode sensitive to tetraphenyl phosphonium and relationship between proton electrochemical potential and phosphorylation potential in steady state. *J. Membr. Biol.* **49,** 105–121 CrossRef Medline
65. Luongo, T. S., Lambert, J. P., Yuan, A., Zhang, X., Gross, P., Song, J., Shanmughapriya, S., Gao, E., Jain, M., Houser, S. R., Koch, W. J., Cheung, J. Y., Madesh, M., and Elrod, J. W. (2015) The mitochondrial calcium uniporter matches energetic supply with cardiac workload during stress and modulates permeability transition. *Cell Rep.* **12,** 23–34 CrossRef Medline
66. Mammucari, C., Gherardi, G., Zamparo, I., Raffaello, A., Boncompagni, S., Chemello, F., Cagnin, S., Braga, A., Zanin, S., Pallafacchina, G., Zentilin, L., Sandri, M., De Stefani, D., Protasi, F., Lanfranchi, G., and Rizzuto, R. (2015) The mitochondrial calcium uniporter controls skeletal muscle trophism *in vivo*. *Cell Rep.* **10,** 1269–1279 CrossRef Medline
67. Kimmich, G. A., Randles, J., and Brand, J. S. (1975) Assay of picomole amounts of ATP, ADP, and AMP using the luciferase enzyme system. *Anal. Biochem.* **69,** 187–206 CrossRef Medline